

15 **Abstract**

16 Climate models generally project an increase in the winter North Atlantic Oscillation (NAO)
17 index under a future high-emissions scenario, alongside an increase in winter precipitation in
18 northern Europe and a decrease in southern Europe. The extent to which future forced NAO
19 trends are important for European winter precipitation trends and their uncertainty remains
20 unclear. We show using the Multimodel Large Ensemble Archive that the NAO plays a small
21 role in northern European mean winter precipitation projections for 2080-2099. Conversely, half
22 of the model uncertainty in southern European mean winter precipitation projections is
23 potentially reducible through improved understanding of the NAO projections. Extreme positive
24 NAO winters increase in frequency in most models as a consequence of mean NAO changes.
25 These extremes also have more severe future precipitation impacts, largely because of mean
26 precipitation changes. This has implications for future resilience to extreme positive NAO
27 winters, which frequently have severe societal impacts.

28

29 **Plain Language Summary**

30 Variations in atmospheric circulation over the North Atlantic are dominated by the North
31 Atlantic Oscillation (NAO) pattern. A positive NAO phase is associated with a northward shift
32 of the North Atlantic storm track, bringing wetter weather to northern Europe and drier weather
33 to southern Europe. In future scenarios with increases in human-caused greenhouse gas
34 emissions, climate models generally simulate an increase in the winter NAO, alongside an
35 increase in winter precipitation in northern Europe and a decrease in southern Europe. However,
36 it is unclear what role the NAO plays in future European winter precipitation trends. Here we
37 show, using a large number of simulations from different climate models, that the NAO plays a
38 small role in late 21st century northern European winter precipitation changes. Conversely, the
39 NAO plays a sizable role in southern Europe. This is important because it suggests that
40 uncertainty in southern European winter precipitation changes could be partly reduced with
41 improved understanding of future NAO changes. Winters with an extremely positive NAO state
42 are generally projected to increase in frequency and have larger precipitation impacts. This has
43 implications for future resilience to these seasonal extremes, which already can have severe
44 societal impacts including flooding and drought.

45 **1 Introduction**

46 The North Atlantic Oscillation (NAO) is the dominant mode of atmospheric circulation
47 variability in the North Atlantic sector and exerts a strong influence on European winter weather
48 and climate (Hurrell et al., 2003). A positive NAO phase is associated with a stronger North
49 Atlantic eddy-driven jet stream and a northward displaced storm track. In winter, this brings mild
50 and wet weather to northern Europe, and cold and dry weather to southern Europe.

51 The NAO is associated with the leading mode of interannual variability in European
52 winter precipitation (Álvarez-García et al., 2019; Qian et al., 2000; Seager et al., 2020; Zveryaev,
53 2006) and can have significant societal impacts. For example, on interannual timescales the
54 NAO influences precipitation and river flows in the Iberian Peninsula, with consequences for
55 water availability for hydroelectricity production and intensive agriculture (Trigo et al., 2004).
56 Prolonged winter periods with a predominantly positive NAO state are also connected to the
57 occurrence of catastrophic flood events in northern Europe, with significant impacts on flood
58 economic losses (Zanardo et al., 2019).

59 On longer timescales, climate models generally project an increase in the winter NAO
60 index by the late 21st century under a high-emissions scenario (Christensen et al., 2013; Gillett &
61 Fyfe, 2013; Lee et al., 2021; Stephenson et al., 2006), alongside an increase in winter
62 precipitation in northern Europe and a decrease in southern Europe (Collins et al., 2013; Lee et
63 al., 2021). While future atmospheric circulation change has been highlighted as a contributor to
64 regional precipitation projections and their uncertainty (Deser et al., 2012, 2017; Fereday et al.,
65 2018; Seager et al., 2010, 2014; Shepherd, 2014; Zappa et al., 2015), the extent to which future
66 forced NAO trends are important for European mean winter precipitation trends and their
67 uncertainty remains unclear. Furthermore, since extreme NAO winters are often associated with
68 detrimental impacts, it is important to determine whether the projected NAO anomaly for the late
69 21st century under high-emissions alters the frequency of extreme positive NAO winters and
70 their associated precipitation.

71 This study aims to determine the role of the NAO for projections of winter European
72 precipitation. Specifically, we address:

- 73 1. What role do modeled forced trends in the NAO play in projections of European
74 mean winter precipitation and their uncertainty?

- 75 2. Do models show an increase in the frequency of extreme positive NAO winters in the
76 future and do mean NAO changes play a role?
- 77 3. Do extreme positive NAO winters have more severe precipitation impacts in the
78 future and do mean NAO changes play a role?

79

80 **2 Methods**

81 2.1 Datasets

82 We use the Multimodel Large Ensemble Archive (MMLEA; Deser et al., 2020). The
83 MMLEA contains large (16-100 member) initial-condition ensembles for seven Coupled Model
84 Intercomparison Project Phase 5 (CMIP5) models (Table S1; Hazeleger et al., 2010; Jeffrey et
85 al., 2013; Kay et al., 2015; Kirchmeier-Young et al., 2017; Maher et al., 2019; Rodgers et al.,
86 2015; Schlunegger et al., 2019; Sun et al., 2018). While CMIP5 models may have stronger
87 precipitation biases than higher resolution models (Roberts et al., 2019), the MMLEA dataset has
88 various unique benefits. Initial-condition large ensembles provide a more accurate measure of
89 the forced climate response and larger samples of relatively rare extreme winters. Multimodel
90 large ensembles also allow us to examine structural model uncertainty in projections (Maher et
91 al., 2021b). The MMLEA models are broadly representative of the spread in CMIP5 projections
92 of the winter NAO index (McKenna & Maycock, 2021) and European winter precipitation
93 (Figure S1), when accounting for internal variability.

94 We use historical and Representative Concentration Pathway (RCP) 8.5 simulations from
95 the MMLEA models for the common period 1950-2099. RCP8.5 was chosen because only a
96 small subset of the models is available for other RCPs. The analysis uses monthly-mean
97 precipitation and mean sea level pressure (MSLP) data averaged over December to February
98 (DJF).

99 The models are evaluated using observation-based MSLP data from the NOAA-CIRES-
100 DOE 20th Century Reanalysis version 3 (20CRv3; Compo et al., 2011; Slivinski et al., 2019).
101 This longer-term dataset was chosen to minimize the sampling errors associated with short
102 observational records. Observed precipitation data is taken from E-OBS version 23.1e (Cornes et

103 al., 2018). We evaluate the models against the observations over a historical period common to
104 all datasets (1951-2014; year is for January).

105 Data are regridded onto a 2° grid using bilinear interpolation for MSLP and a
106 conservative remapping method in Climate Data Operators (Schulzweida, 2021) for
107 precipitation.

108 2.2 Analysis and statistical methods

109 The long-term forced climate response is calculated as the ensemble-mean difference
110 between the end-of-century (2080-2099) and near-present-day (1995-2014).

111 Following Stephenson et al. (2006) and Baker et al. (2018), the NAO index is defined as
112 the difference in area-average MSLP between southern (90°W - 60°E , 20°N - 55°N) and northern
113 (90°W - 60°E , 55°N - 90°N) boxes in the North Atlantic. The results are qualitatively similar for an
114 empirical orthogonal function (EOF)-based NAO index.

115 The NAO-congruent part of a projected pattern of change in precipitation or MSLP is
116 obtained by multiplying the projected change in NAO index by the historical NAO-precipitation
117 or NAO-MSLP pattern. Using a future period to define the patterns gives similar results.
118 Historical NAO-precipitation and NAO-MSLP patterns (Figure S2) are constructed from the
119 regression slopes obtained by regressing historical (1951-2014) timeseries of DJF precipitation
120 and MSLP in each grid-cell onto the NAO timeseries. All timeseries are linearly detrended. For
121 MMLEA models, the patterns are defined for each member and then the ensemble-mean is
122 calculated (Simpson et al., 2020). The modeled and observed NAO-precipitation patterns are
123 highly correlated (Figure S2).

124 Precipitation changes are calculated as a percentage of the modeled 1995-2014
125 climatology. This reduces the influence of model climatological biases: for example, if a model
126 simulates too little precipitation in a region climatologically, it will be unable to simulate a large
127 decrease in precipitation in that region. Since this study concerns the NAO's role in Europe-wide
128 precipitation projections, we calculate the area-average precipitation change over large areas of
129 northern (45°N - 72°N , 10°W - 30°E) and southern (32°N - 45°N , 10°W - 30°E) Europe. These
130 regions are defined based on broad areas of wetting to the north and drying to the south in the
131 multimodel mean (MMM) precipitation projections for MMLEA.

132 95% confidence intervals on the MMLEA results are calculated as follows. For a model
133 ensemble of size N , 10^4 bootstrapped ensembles are created consisting of N members each by
134 resampling with replacement whole ensemble members from the original N -member ensemble.
135 Whole timeseries are sampled to preserve their temporal structure. The given quantity is
136 calculated for each of the 10^4 bootstrapped ensembles and confidence intervals are computed
137 from the spread in the bootstrapped estimates of the quantity.

138

139 **3 Results**

140 3.1 Model evaluation

141 The MMLEA models are first evaluated against observations. Following Thompson et al.
142 (2017), an MMLEA model is said to be indistinguishable from the observations if the observed
143 value of a parameter lies within the 2.5%-97.5% range of inter-member spread in modeled
144 values.

145 Figure S3 evaluates the modeled NAO-precipitation relationships for area-average
146 precipitation in northern and southern Europe. In northern Europe, the observed and modeled
147 relationships are indistinguishable based on the regression slope (Figure S3a) and correlation
148 coefficient (Figure S3b). In southern Europe, however, the models generally simulate too little
149 drying for a positive NAO index anomaly (Figure S3a) and generally underestimate the
150 proportion of total precipitation variability that is NAO-congruent (Figure S3b).

151 Figure S4 evaluates the modeled NAO variability, using summary statistics for the
152 distribution of historical annual winter NAO index anomalies. The standard deviation of the
153 observed winter NAO distribution falls within the inter-member spread for every model except
154 CSIRO-Mk3.6 and EC-EARTH, which have too low variability (Figure S4a). Therefore,
155 CSIRO-Mk3.6 and EC-EARTH are not used for the results on extreme NAO winters (Section
156 3.3). All MMLEA models have a skewness and kurtosis that is indistinguishable from the
157 observations (Figure S4b,c).

158 3.2 Role of the NAO in European mean winter precipitation projections

159 Figure 1a shows the forced change in northern and southern European winter
 160 precipitation between the future and present-day, for each MMLEA model and the MMM. This
 161 is decomposed into an NAO-congruent part and a residual. The models are ordered from left
 162 (CanESM2) to right (GFDL-CM3) with increasing NAO index change. Maps of precipitation
 163 and MSLP change are shown for the MMM in Figure 1b and for each model in Figure S5.

164 In northern Europe, there is a future increase in winter precipitation in all MMLEA
 165 models (Figure 1a). The increase is 15% of the present-day climatology on average and ranges
 166 from 10%-20% across the models. The NAO contribution to the mean change is generally small,
 167 but as expected depends on the magnitude of the NAO trend. For models with the strongest NAO
 168 trends (GFDL-ESM2M, GFDL-CM3), the NAO contributes up to one-third of the mean change
 169 in northern European winter precipitation, but is otherwise small. In all models, the residual
 170 precipitation change accounts for the majority of the total precipitation change.

171 In southern Europe, winter precipitation decreases in the future by an average of 12%
 172 (Figure 1a). However, there is large uncertainty across the models, from no change in CanESM2
 173 to a decrease of 25% in GFDL-CM3. The NAO's role in these precipitation trends is
 174 proportionately larger than for northern Europe, contributing to two-fifths of the total
 175 precipitation change on average and up to half in the model with the largest NAO trend (GFDL-
 176 CM3). There is a residual drying trend in southern Europe in all models, but this only dominates
 177 over the NAO-congruent precipitation change in three models within error (EC-EARTH, MPI-
 178 ESM-LR, GFDL-ESM2M).

179 We now examine the NAO's role for model structural uncertainty in projections of forced
 180 European winter precipitation change. Similar to Fereday et al. (2018), we calculate the fraction
 181 of total intermodel variance in precipitation change that is NAO-congruent as $\sigma_{NAO}^2/\sigma_{TOT}^2$ (Figure
 182 1c), where $\sigma_{TOT}^2 = \sigma_{NAO}^2 + \sigma_{RES}^2$, σ_{NAO}^2 is the intermodel variance in ensemble-mean NAO-
 183 congruent precipitation change, and σ_{RES}^2 is the intermodel variance in ensemble-mean residual
 184 precipitation change (Figure S6). Figure 1c shows the NAO contributes to one-fifth and half of
 185 the intermodel variance in northern and southern European precipitation changes, respectively.
 186 For smaller regions around the dominant centers of action for the NAO-precipitation relationship
 187 (Figure S2), the NAO contributes to a larger proportion of the model uncertainty (Figure 1c).

188 We hypothesize a sizable part of the residual wetting in northern Europe arises from the
189 warming climate and associated increases in specific humidity (Held & Soden, 2006; Manabe &
190 Wetherald, 1980; Seager et al., 2014; Trenberth et al., 2003). Indeed, normalizing precipitation
191 change by global-mean surface air temperature (GSAT) change results in residual and total
192 northern European precipitation changes that are similar in magnitude across the models (Figure
193 S7). While non-NAO-congruent circulation change may play a role in some models (e.g.,
194 CanESM2; Figure S5), there is no clear relationship between the residual circulation and
195 northern European precipitation anomalies on average (Figure 1b). In southern Europe, GSAT
196 change largely does not control the amount of drying (Figure S7; Zappa et al., 2015). On average
197 the residual drying could be associated with non-NAO-congruent anticyclonic circulation
198 anomalies (Figure 1b). Seager et al. (2014) show, however, that near-term future CMIP5-mean
199 Mediterranean precipitation change is both thermodynamic and dynamic in origin.

200 3.3 Frequency and precipitation impacts of future extreme positive NAO winters

201 Anomalous precipitation during extreme positive NAO winters contributes to flooding in
202 northern Europe and meteorological drought in the Iberian Peninsula (Trigo et al., 2004; Zanardo
203 et al., 2019). Figure 2 shows future changes in the frequency of extreme positive NAO winters,
204 defined where the NAO index exceeds the present-day 95th percentile. The model with a negative
205 mean NAO index change (CanESM2) simulates a decrease in frequency of extreme positive
206 NAO winters, while models with positive NAO index changes show increases in frequency of up
207 to 35% (GFDL-CM3). The changes in frequency can be largely explained by the mean NAO
208 index change (Figure 2; Figure S8a). While an increase in NAO variability likely contributes to
209 part of the frequency changes in CESM1-CAM5, changes in NAO variability are not consistent
210 across the MMLEA models (Figure S8b). Changes in the skewness and kurtosis of the annual
211 NAO index distribution are not robust in any model (Figure S8c-d).

212 Figure 3 shows future versus present-day precipitation anomalies (relative to the present-
213 day climatology) for northern and southern Europe during extreme positive NAO winters,
214 defined where the NAO index exceeds the 95th percentile for the given period. For the present-
215 day, extreme positive NAO winters are generally associated with 10% higher winter
216 precipitation in northern Europe and 20% lower precipitation in southern Europe (Figure 3). In
217 the future, all MMLEA models project an increase in wet anomaly in northern Europe during

218 extreme positive NAO winters, from two (MPI-ESM-LR, GFDL-ESM2M) to three times as
219 large (CanESM2, CESM1-CAM5, GFDL-CM3). In southern Europe, models with a smaller
220 mean NAO index change project little change in precipitation (CanESM2, CESM1-CAM5),
221 while models with a larger NAO index change (GFDL-ESM2M, GFDL-CM3) project dry
222 anomalies during strongly positive NAO winters that are around twice as large.

223 A simple explanation for why extreme positive NAO winters have more severe future
224 precipitation impacts is that the shift in climatological mean precipitation causes a shift in
225 precipitation associated with NAO extremes. Future changes in the NAO-precipitation
226 relationship and/or NAO variability could also play a role (e.g., Deser et al., 2017; Osborn,
227 2011).

228 Figure 4 shows the future minus present-day difference in precipitation during extreme
229 positive NAO winters, decomposed into climatological mean parts and an “other” part. The
230 climatological mean changes include the part due to mean NAO index changes and a residual
231 part (i.e., the NAO-congruent part and residual from Figure 1, respectively). This shows
232 precipitation changes during extreme positive NAO winters are largely consistent with
233 climatological mean changes. In northern Europe, the increase in precipitation is dominated by
234 the mean residual changes, a sizable part of which may be associated with background
235 thermodynamic effects in a warmer climate (Section 3.2; Seager et al., 2014). Mean NAO
236 changes play a larger role in southern Europe than for northern Europe, contributing to around
237 half of the total precipitation anomaly in models with larger NAO index changes (GFDL-
238 ESM2M, GFDL-CM3).

239 In CESM1-CAM5 and GFDL-CM3, there is a non-climatological increase and decrease,
240 respectively, in northern European precipitation anomaly during future extreme positive NAO
241 winters, which is different from zero within error. A sizable part of this is explained by an
242 increase and decrease in the NAO-precipitation relationship ($p < 0.05$; not shown), with small
243 contributions from an increase and decrease in interannual NAO variability (Figure S8b).
244 However, projected changes in interannual NAO variability (Figure S8b) and in NAO-
245 precipitation relationship strength (not shown) are not consistent across the MMLEA models.

246

247 **4 Discussion and Conclusions**

248 This study has examined the role of forced NAO changes for projections of winter mean
249 European precipitation using multimodel initial-condition large ensembles from the MMLEA.
250 We use this smaller multimodel ensemble because the CMIP archives typically do not provide
251 enough ensemble members per model to isolate forced NAO changes from internal variability
252 (McKenna & Maycock, 2021).

253 Despite the spread in late 21st century projections of the mean winter NAO index across
254 MMLEA models under the RCP8.5 scenario (McKenna & Maycock, 2021), the pattern of mean
255 winter precipitation change is similar across models with wetting in northern Europe and drying
256 in southern Europe. In northern Europe, the NAO only contributes up to one-third of the
257 precipitation change in a given model and explains one-fifth of the intermodel spread. The NAO
258 plays a larger role in southern Europe, contributing up to half of the precipitation change and
259 explaining half of the intermodel spread. The NAO is relatively more important for precipitation
260 change in certain smaller regions, including northwest Europe and the Iberian Peninsula, than at
261 a continental scale.

262 Stephenson et al. (2006) found the NAO plays little role in mean winter precipitation
263 projections for both northern and southern Europe. A direct comparison with our results is
264 difficult, however, because they: 1) used an early generation of climate models (CMIP2); 2) had
265 only one ensemble member available per model; and 3) analyzed idealized CO₂-only forcing
266 simulations. In southern Europe or the Mediterranean, Zappa et al. (2015) and Fereday et al.
267 (2018) show that future atmospheric circulation change contributes >50% of the CMIP5-mean
268 winter precipitation response and 75%-80% of the intermodel spread. Our results suggest a large
269 part of the forced component of the spread could be reduced by better understanding the causes
270 of model uncertainty in NAO projections. In northern Europe, Fereday et al. (2018) also find
271 little role of future atmospheric circulation change for CMIP5-mean winter precipitation change,
272 but there is larger intermodel spread from circulation than found here. This discrepancy partly
273 reflects that we specifically consider NAO-congruent circulation changes and, also, intermodel
274 spread in CMIP5 precipitation projections is inflated by internal variability in atmospheric
275 circulation, which the MMLEA models reduce (Deser et al., 2017; Figure S1). The additional

276 spread in Fereday et al. (2018)'s northern European precipitation projections arises from their
277 use of monthly rather than seasonal trends and different methodological choices (e.g., expressing
278 precipitation changes relative to the E-OBS climatology).

279 Second, we examine future changes in the frequency of extreme positive ($\geq 95^{\text{th}}$
280 percentile) NAO winters, which are often associated with severe societal impacts. The MMLEA
281 models generally project an increase in extreme positive NAO winter frequency, largely due to a
282 positive shift in mean NAO index. The increase can be up to 35% – i.e., a 1-in-20 year winter
283 becomes a 2-in-5 year winter – but large intermodel spread in the magnitude of mean NAO index
284 changes results in large model uncertainty in extreme frequency changes.

285 Third, we show extreme positive NAO winters have more severe precipitation impacts in
286 future in all MMLEA models. In particular, future extreme positive NAO winters have northern
287 European wet anomalies that are two to three times larger than in the present-day and southern
288 European dry anomalies that are up to two times larger. Mean NAO index changes contribute up
289 to half of the southern European precipitation changes. Across the MMLEA models, however,
290 the most robust Europe-wide contribution is from non-NAO-congruent changes in climatological
291 winter precipitation. Specifically, the larger precipitation anomalies during future extreme
292 positive NAO winters arise from NAO-induced precipitation anomalies similar to present-day,
293 superposed onto a future background climatology that constructively interferes with the NAO-
294 precipitation pattern. This result implies a future decrease in our resilience to this type of
295 seasonal extreme, which can already have severe societal impacts. This is an important
296 consideration for policymakers involved in climate adaptation.

297 Model biases could influence this study's results. For example, the MMLEA models may
298 underestimate NAO-congruent changes in southern European precipitation given the too-weak
299 NAO-precipitation relationship in this region. They may also underestimate future increases in
300 northern European precipitation as compared to higher resolution models (Moreno-Chamarro et
301 al., 2021). Multiple Regional Climate Model initial-condition large ensembles are now becoming
302 available (Maher et al., 2021a), which could be used to further examine the influence of biases.
303 Importantly, models have been shown to underestimate forced NAO variability by a factor of
304 two on seasonal timescales (Baker et al., 2018; Dunstone et al., 2016; Eade et al., 2014; Scaife &
305 Smith, 2018; Scaife et al., 2014) and ten on decadal timescales (Smith et al., 2020). If models

306 also underestimate multidecadal forced NAO variability, late 21st century NAO-congruent
307 changes in European winter mean precipitation may be underestimated. Future work should
308 examine whether modeled multidecadal NAO variability has a too-low signal-to-noise ratio.
309 Understanding the mechanisms responsible for intermodel spread in future forced NAO changes
310 could provide an important constraint on the spread in southern European mean winter
311 precipitation projections.

312

313 **Acknowledgments**

314 CMM and ACM were supported by the European Union's Horizon 2020 research and innovation
315 programme under grant agreement No 820829 (CONSTRAIN project). ACM was supported by
316 The Leverhulme Trust. We acknowledge the U.S. CLIVAR Working Group on Large Ensembles
317 for providing the MMLEA data, the E-OBS dataset from the EU-FP6 project UERRA
318 (<https://www.uerra.eu>) and the Copernicus Climate Change Service, and the data providers in the
319 ECA&D project (<https://www.ecad.eu>). We acknowledge the World Climate Research
320 Programme's Working Group on Coupled Modelling, which is responsible for CMIP, and thank
321 the climate modeling groups (see Table S2) for producing and making available their model
322 output. For CMIP the U.S. Department of Energy's Program for Climate Model Diagnosis and
323 Intercomparison provides coordinating support and led development of software infrastructure in
324 partnership with the Global Organization for Earth System Science Portals.

325

326 **Data Availability Statement**

327 The Multimodel Large Ensemble Archive data can be accessed at
328 <http://www.cesm.ucar.edu/projects/community-projects/MMLEA/>. The GFDL-ESM2M large
329 ensemble data used here can be accessed from the Princeton Large Ensemble Archive through
330 Globus (<https://www.sarahschlunegger.com/large-ensemble-archive>). 20CRv3 can be
331 downloaded from https://psl.noaa.gov/data/gridded/data.20thC_ReanV3.html and E-OBS from
332 https://surfobs.climate.copernicus.eu/dataaccess/access_eobs.php. The CMIP5 precipitation data
333 were downloaded from CEDA/JASMIN (timestamp of 23 May 2022); these are publicly

334 available through the Earth System Grid Federation at [https://esgf-
index1.ceda.ac.uk/projects/cmip5-ceda/](https://esgf-
335 index1.ceda.ac.uk/projects/cmip5-ceda/).

336

337 **References**

338 Álvarez-García, F. J., OrtizBevia, M. J., Cabos, W., Tasambay-Salazar, M., & RuizdeElvira, A.
339 (2019). Linear and nonlinear links of winter European precipitation to Northern
340 Hemisphere circulation patterns. *Climate Dynamics*, *52*, 6533–6555.
341 <https://doi.org/10.1007/s00382-018-4531-6>

342 Baker, L. H., Shaffrey, L. C., Sutton, R. T., Weisheimer, A., & Scaife, A. A. (2018). An
343 intercomparison of skill and overconfidence/underconfidence of the wintertime North
344 Atlantic Oscillation in multimodel seasonal forecasts. *Geophysical Research Letters*, *45*,
345 7808–7817. <https://doi.org/10.1029/2018GL078838>

346 Christensen, J. H., Krishna Kumar, K., Aldrian, E., An, S. -I., Cavalcanti, I. F. A., de Castro, M.,
347 et al. (2013). Climate Phenomena and their Relevance for Future Regional Climate
348 Change. In T. F. Stocker, et al. (Eds.), *Climate Change 2013: The Physical Science Basis. Contribution of Working Group I to the Fifth Assessment Report of the Intergovernmental Panel on Climate Change* (pp. 1217–1308). Cambridge, UK, and New York, NY, USA: Cambridge University Press. <https://doi.org/10.1017/CBO9781107415324.028>

352 Compo, G. P., Whitaker, J. S., Sardeshmukh, P. D., Matsui, N., Allan, R. J., Yin, X., et al.
353 (2011). The Twentieth Century Reanalysis Project. *Quarterly Journal of the Royal Meteorological Society*, *137*(654), 1–28. <https://doi.org/10.1002/qj.776>

355 Cornes, R., van der Schrier, G., van den Besselaar, E. J. M., & Jones, P. D. (2018). An Ensemble
356 Version of the E-OBS Temperature and Precipitation Datasets. *Journal of Geophysical Research: Atmospheres*, *123*(17), 9391–9409. <https://doi.org/10.1029/2017JD028200>

358 Deser, C., Hurrell, J. W., & Phillips, A. S. (2017). The role of the North Atlantic Oscillation in
359 European climate projections. *Climate Dynamics*, *49*, 3141–3157.
360 <https://doi.org/10.1007/s00382-016-3502-z>

- 361 Deser, C., Lehner, F., Rodgers, K. B., Ault, T., Delworth, T. L., DiNezio, P. N., et al. (2020).
362 Insights from Earth system model initial-condition large ensembles and future prospects.
363 *Nature Climate Change*, 10, 277–286. <https://doi.org/10.1038/s41558-020-0731-2>
- 364 Deser, C., Phillips, A., Bourdette, V., & Teng, H. (2012). Uncertainty in climate change
365 projections: the role of internal variability. *Climate Dynamics*, 38, 527–546.
366 <https://doi.org/10.1007/s00382-010-0977-x>
- 367 Dunstone, N., Smith, D., Scaife, A., Hermanson, L., Eade, R., Robinson, N., et al. (2016). Skilful
368 predictions of the winter North Atlantic Oscillation one year ahead. *Nature Geoscience*,
369 9, 809–814. <https://doi.org/10.1038/ngeo2824>
- 370 Eade, R., Smith, D., Scaife, A., Wallace, E., Dunstone, N., Hermanson, L., & Robinson, N.
371 (2014). Do seasonal-to-decadal climate predictions underestimate the predictability of the
372 real world? *Geophysical Research Letters*, 41(15), 5620–5628.
373 <https://doi.org/10.1002/2014GL061146>
- 374 Fereday, D., Chadwick, R., Knight, J., & Scaife, A. A. (2018). Atmospheric Dynamics is the
375 Largest Source of Uncertainty in Future Winter European Rainfall. *Journal of Climate*,
376 31(3), 963–977. <https://doi.org/10.1175/JCLI-D-17-0048.1>
- 377 Gillett, N. P., & Fyfe, J. C. (2013). Annular mode changes in the CMIP5 simulations.
378 *Geophysical Research Letters*, 40(6), 1189–1193. <https://doi.org/10.1002/grl.50249>
- 379 Hazeleger, W., Severijns, C., Semmler, T., Ștefănescu, S., Yang, S., Wang, X., et al. (2010). EC-
380 Earth. *Bulletin of the American Meteorological Society*, 91(10), 1357–1364.
381 <https://doi.org/10.1175/2010BAMS2877.1>
- 382 Held, I. M., & Soden, B. J. (2006). Robust Responses of the Hydrological Cycle to Global
383 Warming. *Journal of Climate*, 19(21), 5686–5699. <https://doi.org/10.1175/JCLI3990.1>
- 384 Hurrell, J. W., Kushnir, Y., Ottersen, G., & Visbeck, M. (2003). An overview of the North
385 Atlantic Oscillation. In J. W. Hurrell, Y., et al. (Eds.), *The North Atlantic Oscillation:
386 Climate Significance and Environmental Impact*, *Geophysical Monograph Series* (Vol.

- 387 134, pp. 1–35). Washington, DC: American Geophysical Union.
388 <https://doi.org/10.1029/134GM01>
- 389 Jeffrey, S., Rotstayn, L., Collier, M., Dravitzki, S., Hamalainen, C., Moeseneder, C., et al.
390 (2013). Australia's CMIP5 submission using the CSIRO-Mk3.6 model. *Australian*
391 *Meteorological and Oceanographic Journal*, 63(1), 1–14.
392 <https://doi.org/10.22499/2.6301.001>
- 393 Kay, J. E., Deser, C., Phillips, A., Mai, A., Hannay, C., Strand, G., et al. (2015). The Community
394 Earth System Model (CESM) Large Ensemble project: A community resource for
395 studying climate change in the presence of internal climate variability. *Bulletin of the*
396 *American Meteorological Society*, 96(8), 1333–1349. [https://doi.org/10.1175/BAMS-D-](https://doi.org/10.1175/BAMS-D-13-00255.1)
397 [13-00255.1](https://doi.org/10.1175/BAMS-D-13-00255.1)
- 398 Kirchmeier-Young, M. C., Zwiers, F. W., & Gillett, N. P. (2017). Attribution of extreme events
399 in Arctic sea ice extent. *Journal of Climate*, 30(2), 553–571.
400 <https://doi.org/10.1175/JCLI-D-16-0412.1>
- 401 Lee, J. -Y., Marotzke, J., Bala, G., Cao, L., Corti, S., Dunne, J. P., et al. (2021). Future Global
402 Climate: Scenario-Based Projections and Near-Term Information. In Masson-Delmotte,
403 V., et al. (Eds.), *Climate Change 2021: The Physical Science Basis. Contribution of*
404 *Working Group I to the Sixth Assessment Report of the Intergovernmental Panel on*
405 *Climate Change* (pp. 553–672). Cambridge, UK, and New York, NY, USA: Cambridge
406 University Press. <https://doi.org/10.1017/9781009157896.006>
- 407 Maher, N., Milinski, S., & Ludwig, R. (2021a). Large ensemble climate model simulations:
408 introduction, overview, and future prospects for utilising multiple types of large
409 ensemble. *Earth System Dynamics*, 12, 401–418. [https://doi.org/10.5194/esd-12-401-](https://doi.org/10.5194/esd-12-401-2021)
410 [2021](https://doi.org/10.5194/esd-12-401-2021)
- 411 Maher, N., Milinski, S., Suarez-Gutierrez, L., Botzet, M., Dobrynin, M., Kornblueh, L., et al.
412 (2019). The Max Planck Institute Grand Ensemble: Enabling the exploration of climate
413 system variability. *Journal of Advances in Modeling Earth Systems*, 11(7), 2050–2069.
414 <https://doi.org/10.1029/2019MS001639>

- 415 Maher, N., Power, S. B., & Marotzke, J. (2021b). More accurate quantification of model-to-
416 model agreement in externally forced climatic responses over the coming century. *Nature*
417 *Communications*, 12, 788. <https://doi.org/10.1038/s41467-020-20635-w>
- 418 Manabe, S., & Wetherald, R. T. (1980). On the Distribution of Climate Change Resulting from
419 an Increase in CO₂ Content of the Atmosphere. *Journal of Atmospheric Sciences*, 37(1),
420 99–118. [https://doi.org/10.1175/1520-0469\(1980\)037<0099:OTDOCC>2.0.CO;2](https://doi.org/10.1175/1520-0469(1980)037<0099:OTDOCC>2.0.CO;2)
- 421 McKenna, C. M., & Maycock, A. C. (2021). Sources of uncertainty in Multimodel Large
422 Ensemble projections of the winter North Atlantic Oscillation. *Geophysical Research*
423 *Letters*, 48(14), e2021GL093258. <https://doi.org/10.1029/2021GL093258>
- 424 Moreno-Chamarro, E., Caron, L. P., Ortega, P., Tomas, S. L., & Roberts, M. J. (2021). Can we
425 trust CMIP5/6 future projections of European winter precipitation? *Environmental*
426 *Research Letters*, 16(5), 054063. <https://doi.org/10.1088/1748-9326/abf28a>
- 427 Osborn T. J. (2011). Variability and Changes in the North Atlantic Oscillation Index. In Vicente-
428 Serrano S., Trigo R. (Eds.), *Hydrological, Socioeconomic and Ecological Impacts of the*
429 *North Atlantic Oscillation in the Mediterranean Region. Advances in Global Change*
430 *Research* (Vol. 46, pp. 9–22). Dordrecht, Netherlands: Springer.
431 https://doi.org/10.1007/978-94-007-1372-7_2
- 432 Qian, B., Corte-Real, J., & Xu, H. (2000). Is the North Atlantic Oscillation the most important
433 atmospheric pattern for precipitation in Europe? *Journal of Geophysical Research:*
434 *Atmospheres*, 105(D9), 11901–11910. <https://doi.org/10.1029/2000JD900102>
- 435 Roberts, M. J., Baker, A., Blockley, E. W., Calvert, D., Coward, A., Hewitt, H. T., et al. (2019).
436 Description of the resolution hierarchy of the global coupled HadGEM3-GC3.1 model as
437 used in CMIP6 HighResMIP experiments. *Geoscientific Model Developments*, 12(12),
438 4999–5028. <https://doi.org/10.5194/gmd-12-4999-2019>
- 439 Rodgers, K. B., Lin, J., & Frölicher, T. L. (2015). Emergence of multiple ocean ecosystem
440 drivers in a large ensemble suite with an Earth system model. *Biogeosciences*, 12(11),
441 3301–3320. <https://doi.org/10.5194/bg-12-3301-2015>

- 442 Scaife, A. A., Arribas, A., Blockley, E., Brookshaw, A., Clark, R. T., Dunstone, N., et al. (2014).
443 Skillful long-range prediction of European and North American winters. *Geophysical*
444 *Research Letters*, 41(7), 2514–2519. <https://doi.org/10.1002/2014GL059637>
- 445 Scaife, A. A., & Smith, D. (2018). A signal-to-noise paradox in climate science. *npj Climate and*
446 *Atmospheric Science*, 1, 28. <https://doi.org/10.1038/s41612-018-0038-4>
- 447 Schlunegger, S., Rodgers, K. B., Sarmiento, J. L., Frölicher, T. L., Dunne, J. P., Ishii, M., &
448 Slater, R. (2019). Emergence of anthropogenic signals in the ocean carbon cycle. *Nature*
449 *Climate Change*, 9, 719–725. <https://doi.org/10.1038/s41558-019-0553-2>
- 450 Schulzweida, Uwe. (2021). CDO User Guide (Version 2.0.0). Zenodo.
451 <http://doi.org/10.5281/zenodo.5614769>
- 452 Seager, R., Liu, H., Henderson, N., Simpson, I., Kelley, C., Shaw, T., et al. (2014). Causes of
453 Increasing Aridification of the Mediterranean Region in Response to Rising Greenhouse
454 Gases. *Journal of Climate*, 27(12), 4655–4676. [https://doi.org/10.1175/JCLI-D-13-](https://doi.org/10.1175/JCLI-D-13-00446.1)
455 [00446.1](https://doi.org/10.1175/JCLI-D-13-00446.1)
- 456 Seager, R., Liu, H., Kushnir, Y., Osborn, T. J., Simpson, I. R., Kelley, C. R., & Nakamura, J.
457 (2020). Mechanisms of Winter Precipitation Variability in the European–Mediterranean
458 Region Associated with the North Atlantic Oscillation. *Journal of Climate*, 33(16), 7179–
459 7196. <https://doi.org/10.1175/JCLI-D-20-0011.1>
- 460 Seager, R., Naik, N., & Vecchi, G. A. (2010). Thermodynamic and Dynamic Mechanisms for
461 Large-Scale Changes in the Hydrological Cycle in Response to Global Warming. *Journal*
462 *of Climate*, 23(17), 4651–4668. <https://doi.org/10.1175/2010JCLI3655.1>
- 463 Shepherd, T. (2014). Atmospheric circulation as a source of uncertainty in climate change
464 projections. *Nature Geoscience*, 7, 703–708. <https://doi.org/10.1038/ngeo2253>
- 465 Slivinski, L. C., Compo, G. P., Whitaker, J. S., Sardeshmukh, P. D., Giese, B. S., McColl, C., et
466 al. (2019). Towards a more reliable historical reanalysis: Improvements for version 3 of
467 the Twentieth Century Reanalysis system. *Quarterly Journal of the Royal Meteorological*
468 *Society*, 145(724), 2876–2908. <https://doi.org/10.1002/qj.3598>

- 469 Smith, D. M., Scaife, A. A., Eade, R., Athanasiadis, P., Bellucci, A., Bethke, I., et al. (2020).
470 North Atlantic climate far more predictable than models imply. *Nature*, 583, 796–800.
471 <https://doi.org/10.1038/s41586-020-2525-0>
- 472 Stephenson, D., Pavan, V., Collins, M., Junge, M., Quadrelli, R., & Participating CMIP2
473 Modelling Groups (2006). North Atlantic Oscillation response to transient greenhouse
474 gas forcing and the impact on European winter climate: A CMIP2 multi-model
475 assessment. *Climate Dynamics*, 27(4), 401–420. [https://doi.org/10.1007/s00382-006-](https://doi.org/10.1007/s00382-006-0140-x)
476 [0140-x](https://doi.org/10.1007/s00382-006-0140-x)
- 477 Sun, L., Alexander, M., & Deser, C. (2018). Evolution of the global coupled climate response to
478 Arctic Sea ice loss during 1990–2090 and its contribution to climate change. *Journal of*
479 *Climate*, 31(19), 7823–7843. <https://doi.org/10.1175/JCLI-D-18-0134.1>
- 480 Thompson, V., Dunstone, N. J., Scaife, A. A., Smith, D. M., Slingo, J. M., Brown, S., & Belcher,
481 S. E. (2017). High risk of unprecedented UK rainfall in the current climate. *Nature*
482 *Communications*, 8, 107. <https://doi.org/10.1038/s41467-017-00275-3>
- 483 Trenberth, K. E., Dai, A., Rasmussen, R. M., & Parsons, D. B. (2003). The Changing Character
484 of Precipitation. *Bulletin of the American Meteorological Society*, 84(9), 1205–1218.
485 <https://doi.org/10.1175/BAMS-84-9-1205>
- 486 Trigo, R. M., Pozo-Vázquez, D., Osborn, T. J., Castro-Díez, Y., Gámiz-Fortis, S., & Esteban-
487 Parra, M. J. (2004). North Atlantic Oscillation influence on precipitation, river flow and
488 water resources in the Iberian Peninsula. *International Journal of Climatology*, 24(8),
489 925–944. <https://doi.org/10.1002/joc.1048>
- 490 Zanardo, S., Nicotina, L., Hilberts, A. G. J., & Jewson, S. P. (2019). Modulation of economic
491 losses from European floods by the North Atlantic Oscillation. *Geophysical Research*
492 *Letters*, 46(5), 2563–2572. <https://doi.org/10.1029/2019GL081956>
- 493 Zappa, G., Hoskins, B. J., & Shepherd, T. G. (2015). The dependence of wintertime
494 Mediterranean precipitation on the atmospheric circulation response to climate change.

495 *Environmental Research Letters*, 10(10), 104012. [https://doi.org/10.1088/1748-](https://doi.org/10.1088/1748-9326/10/10/104012)
496 [9326/10/10/104012](https://doi.org/10.1088/1748-9326/10/10/104012)

497 Zveryaev, I. I. (2006). Seasonally varying modes in long-term variability of European
498 precipitation during the 20th century. *Journal of Geophysical Research*, 111, D21116.
499 <https://doi.org/10.1029/2005JD006821>

500

501 **Figure captions**

502 **Figure 1:** Role of forced DJF NAO index change (Δ NAOI) in DJF precipitation projections
503 (2080-2099 minus 1995-2014) for the MMLEA models. (a) Area-average precipitation
504 anomalies in northern (blue) and southern (brown) Europe; regions are defined by blue and
505 brown boxes in (b). Left bar: Total anomaly; Middle bar: NAO-congruent part; Right bar:
506 Residual. Precipitation anomalies are shown as a percentage of the 1995-2014 climatology. Error
507 bars show bootstrapped 95% confidence intervals. (b) Maps of multimodel mean (MMM)
508 precipitation (shading) and MSLP (contours) anomalies; Figure S5 shows maps for each model.
509 Contours range from -2 hPa (dashed) to 2 hPa (solid) in 1 hPa intervals. (c) Fraction of total
510 intermodel variance in precipitation projections that is NAO-congruent; see Figure S6 for further
511 explanation. Colored numbers indicate fractions for northern and southern European
512 precipitation changes in (a).

513 **Figure 2:** Projected change (2080-2099 minus 1995-2014) in the frequency of extreme positive
514 ($\geq 95^{\text{th}}$ percentile for 1995-2014) NAO winters for selected MMLEA models (see Section 3.1).
515 Contribution of mean DJF NAO index change (Δ NAOI) is calculated by shifting the 1995-2014
516 distribution of annual DJF NAO index by Δ NAOI. Error bars show bootstrapped 95%
517 confidence intervals.

518 **Figure 3:** Precipitation anomalies during extreme positive ($\geq 95^{\text{th}}$ percentile) NAO winters for
519 2080-2099 versus 1995-2014 in selected MMLEA models (see Section 3.1). (a) Area-average
520 precipitation anomalies in northern (blue) and southern (brown) Europe; regions are defined by
521 blue and brown boxes in (b). Left bar: 1995-2014 anomaly; Middle bar: 2080-2099 anomaly;
522 Right bar: 2080-2099 anomaly minus 1995-2014 anomaly. Precipitation anomalies are shown as

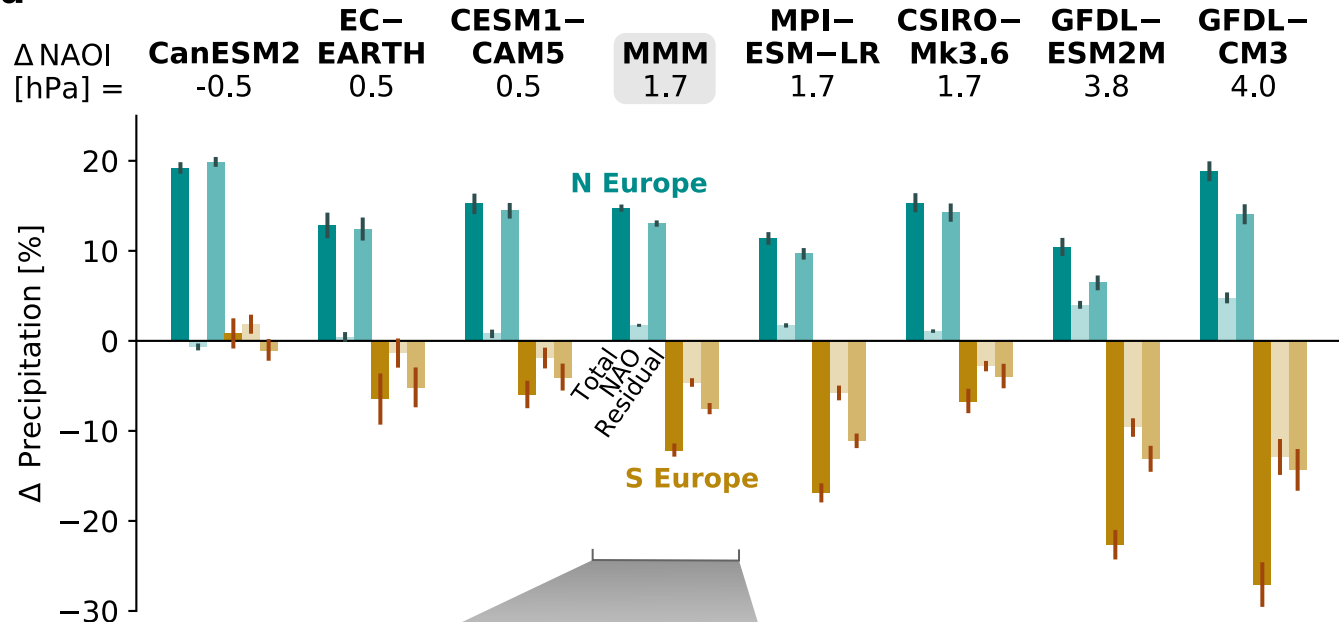
523 a percentage of the 1995-2014 climatology and averaged over all extreme positive NAO winters.
524 Error bars show bootstrapped 95% confidence intervals. Δ NAOI is the mean DJF NAO index
525 change for 2080-2099 minus 1995-2014. The multimodel mean (MMM) is for the selected
526 models only. (b) Maps of MMM precipitation (shading) and MSLP (contours) anomalies; Figure
527 S9 shows maps for each model. Contours range from -10.5 hPa (dashed) to 6 hPa (solid) in 1.5
528 hPa intervals.

529 **Figure 4:** Decomposition of projected precipitation change (2080-2099 minus 1995-2014)
530 during extreme positive ($\geq 95^{\text{th}}$ percentile) NAO winters in selected MMLEA models (see
531 Section 3.1). (a) Area-average precipitation anomalies in northern (blue) and southern (brown)
532 Europe; regions are defined by blue and brown boxes in (b). Far left bar: Total anomaly; Middle
533 left bar: Part from mean DJF NAO index change (Δ NAOI, NAO part in Figure 1); Middle right
534 bar: Part from mean residual change (residual in Figure 1); Far right bar: Non-climatological
535 “other” part. Precipitation anomalies are shown as a percentage of the 1995-2014 climatology
536 and averaged over all extreme positive NAO winters. Error bars show bootstrapped 95%
537 confidence intervals. The multimodel mean (MMM) is for the selected models only. (b) Maps of
538 MMM precipitation (shading) and MSLP (contours) anomalies. Contours range from -2 hPa
539 (dashed) to 1 hPa (solid) in 1 hPa intervals.

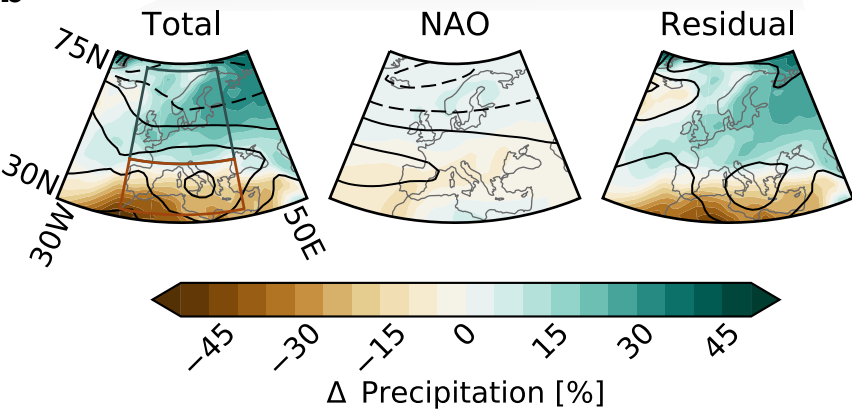
Figure 1.

Role of NAO in DJF precipitation change, [2080-2099] – [1995-2014]

a



b



c

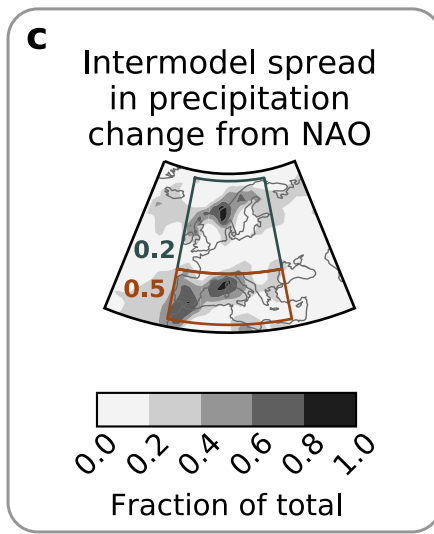


Figure 2.

Projected change in frequency of extreme ($\geq 95^{\text{th}}$ PC) DJF NAO+ years

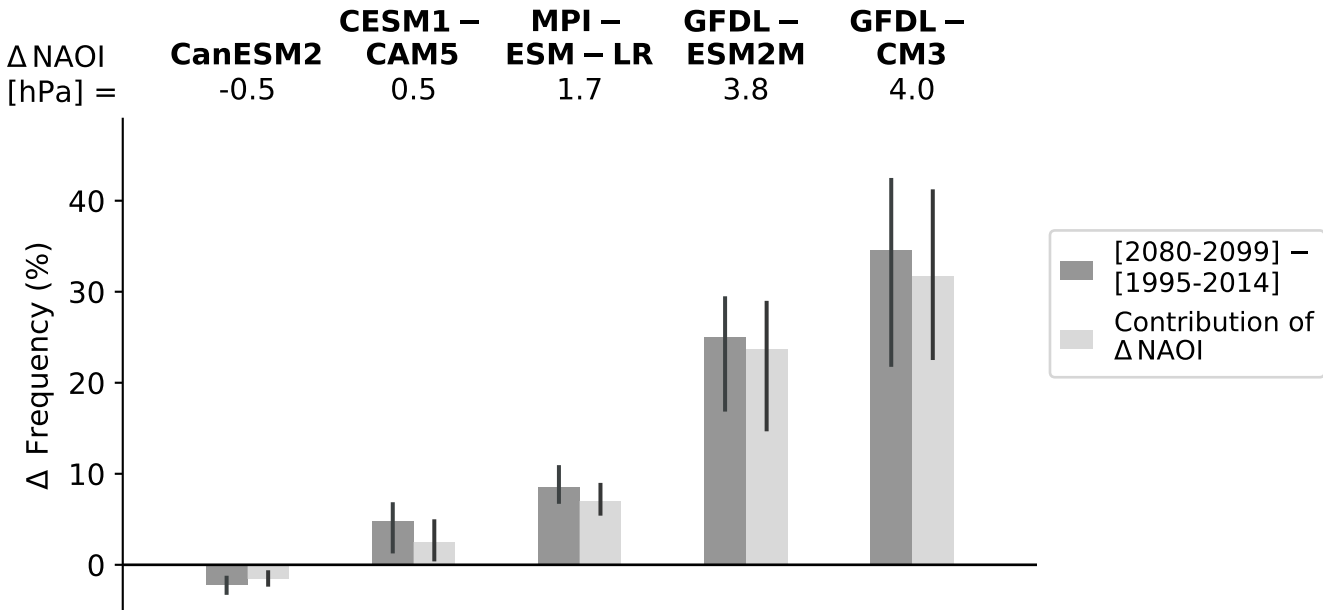
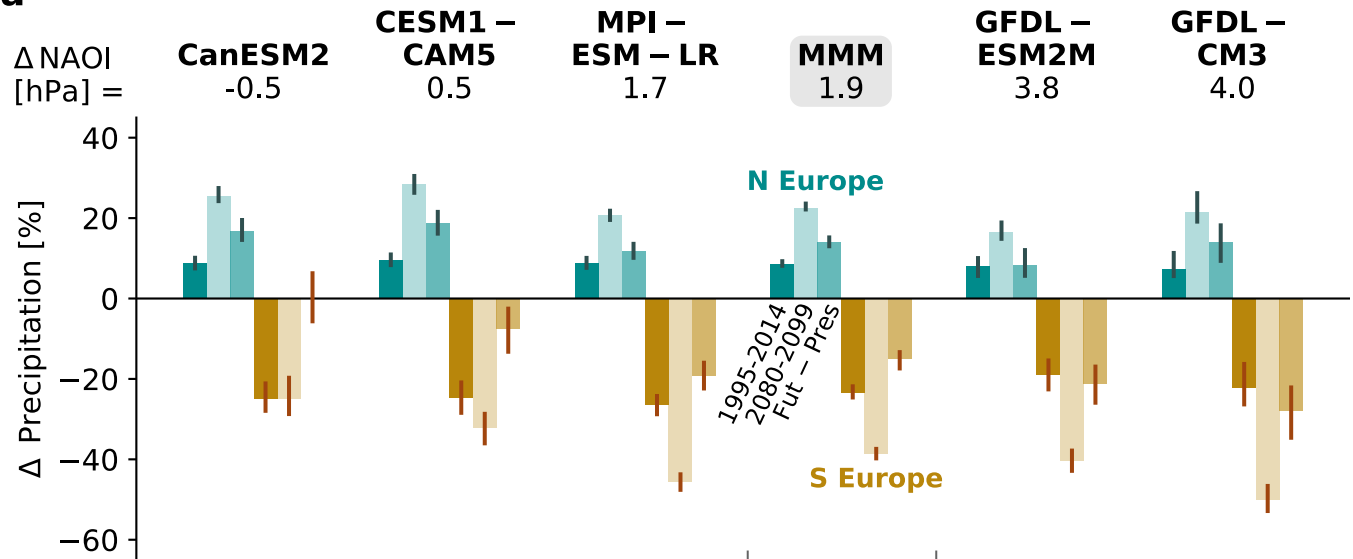


Figure 3.

Precipitation anomalies in extreme ($\geq 95^{\text{th}}$ PC) DJF NAO+ years

a



b

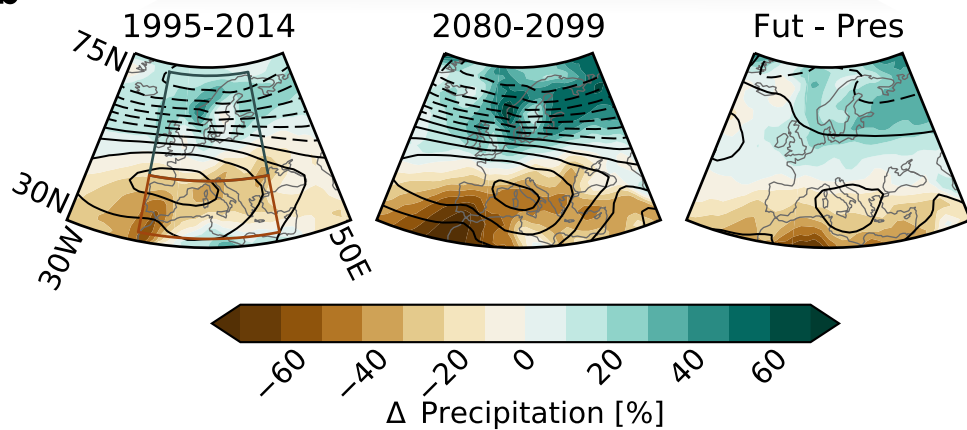
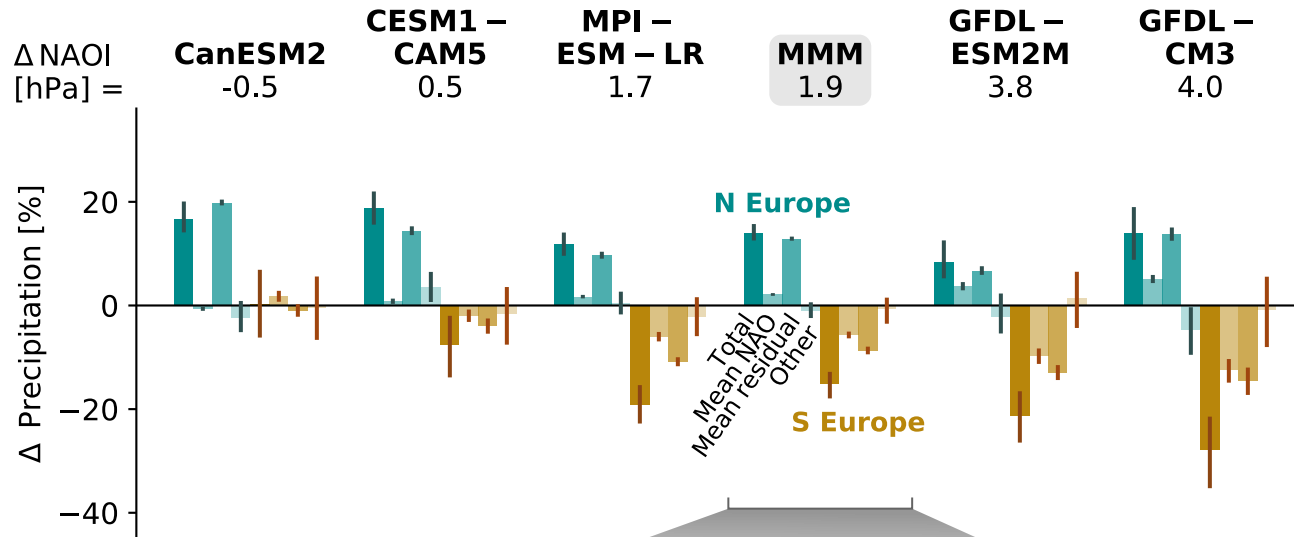


Figure 4.

Decomposition of precipitation projections for extreme ($\geq 95^{\text{th}}$ PC) DJF NAO+ years, [2080-2099] – [1995-2014]

a



b

